Improvements in fundamental performance of liquid-environment atomic force microscopy with true atomic resolution

doi: 10.7567/JJAP.54.08LA03

Improvements in fundamental performance of liquid-environment atomic force microscopy with true atomic resolution

Kazuki Miyata[1], Keisuke Miyazawa[1], Seyed Mohammad Reza Akrami[1] and Takeshi Fukuma[*1,2]

[1]*Division of Electrical Engineering and Computer Science, Kanazawa University, Kanazawa 920-1192, Japan*

[2]*ACT-C, Japan Science and Technology Agency, Saitama 332-0012, Japan*

Recently, there have been significant advancements in liquid-environment atomic force microscopy (AFM) with true atomic resolution. The technical advancements are followed by a rapid expansion of its application area. Examples include subnanometer-scale imaging of biological systems and three-dimensional measurements of water distributions (i.e., hydration structures) and fluctuating surface structures. However, to continue this progress, we should improve the fundamental performance of liquid-environment dynamic-mode AFM. The present AFM technique does not allow real-time imaging of atomic-scale dynamic phenomena at a solid-liquid interface. This has hindered atomic-level understanding of crystal growth and dissolution, catalytic reactions and metal corrosion processes. Improvement in force sensitivity is required not only for such a high-speed imaging but also for various surface property measurements using a high-resolution AFM technique. In this review, we summarize recent works on the improvements in the force sensitivity and operation speed of atomic-resolution dynamic-mode AFM for liquid-environment applications.

1. Introduction

Atomic-scale processes at a solid-liquid interface play important roles in chemical reactions on an electrode or a catalyst, and molecular interactions at a biomolecular interface. However, difficulties in direct imaging of these processes have hindered their atomic-scale understanding. Atomic force microscopy (AFM)[1)] is one of the most promising candidates to solve this problem. In 1993, Ohnesorge and Binnig first demonstrated true atomic-resolution imaging in liquid by static-mode AFM.[2)] However, static-mode AFM imaging often damaged a sample owing to the lateral scan of a tip in contact with a surface.

Recently, there have been significant advancements in liquid-environment dynamic-mode AFM. In 2005, Fukuma *et al.* demonstrated true atomic-resolution imaging in

*E-mail: fukuma@staff.kanazawa-u.ac.jp

liquid by frequency modulation AFM (FM-AFM).[3] Subsequently, a comparable spatial resolution was also achieved by other operation modes such as phase modulation and amplitude modulation AFMs (PM- and AM-AFMs).[4,5] One of the key techniques that enabled high-resolution imaging is small-amplitude oscillation of a cantilever ($A <$ 0.5 nm). The reduction of A enhances sensitivity to a short-range interaction force,[6] which enabled true atomic-resolution imaging even with a low Q factor of the cantilever resonance.

The progress in liquid-environment dynamic-mode AFM opened up possibilities of various imaging studies. Examples include subnanometer-scale imaging of biological systems under physiologically relevant solution conditions,[7–10] and direct visualization of three-dimensional (3D) distributions of hydration structures,[11,12] and flexible molecular chains.[13] These advanced applications highlighted the excellent potential of high-resolution AFM in liquid.

To continue this progress, it is essential to improve the fundamental performance of liquid-environment dynamic-mode AFM. Direct imaging of dynamic phenomena such as molecular interactions, crystal growth and dissolution, catalytic reactions and corrosion processes requires a wide bandwidth for tip-sample distance regulation. To increase the bandwidth without deteriorating the present spatial resolution, we should also improve the force sensitivity. In this review, we summarize recent works on the improvements in the force sensitivity and operation speed of liquid-environment high-resolution AFM.

2. Improvement of force sensitivity

To obtain a true atomic-resolution image by AFM, we typically need to visualize ∼10 pm corrugations. At a solid-liquid interface, the tip-sample distance is regulated at a force branch with a slope of ∼1 N/m. Thus, the minimum detectable force (F_{min}) required for true atomic-resolution imaging is typically ∼10 pN. For visualizing 3D hydration structures at a solid-liquid interface, we should, at least, detect force variations caused by the first and second hydration shells. For the first hydration shell, the induced force variation is a few hundreds of piconewtons, while that for the second hydration shell is several tens of piconewtons. Therefore, 3D hydration structure imaging also requires ∼10 pN F_{min}. The present AFM can barely satisfy these requirements. The limited performance margin leads to poor reproducibility and strong dependence on the user skills. In addition, it also limits the measurement bandwidth to less than 100 Hz. In the rest of this section, we describe recent works to overcome this limitation by improving

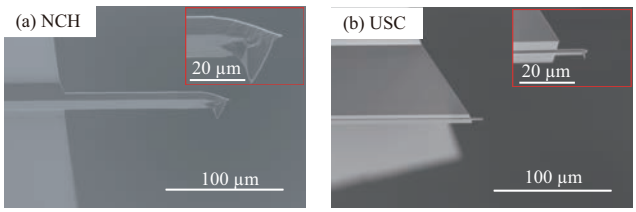

Fig. 1. (Color online) SEM images of (a) conventional (NCH) and (b) small cantilevers. Reused with permission from Ref. 18. Copyright 2012 IOP Publishing.

F_{min}.

2.1 Small cantilevers for improving minimum detectable force

F_{min} in dynamic-mode AFM is ultimately determined by the thermal vibration of a cantilever. With the small amplitude approximation, F_{min} for FM- and PM-AFM is given by[4,14]

$$F_{\mathrm{min}} = \sqrt{\frac{4kk_BTB}{\pi f_0 Q}}, \tag{1}$$

where k, Q, f_0, k_B, and T denote the spring constant, Q factor and resonance frequency of a cantilever, Boltzmann's constant, and temperature, respectively. For AM-AFM, F_{min} depends on the position of the cantilever driving frequency relative to the cantilever resonance. However, the optimal value is given by an equation similar to Eq. (1).[15]

Among the parameters in Eq. (1), T and B are typically determined by the application purpose. Thus, we cannot arbitrarily change the values for improving F_{min}. The reduction in k generally leads to an increase in instability such as that caused by thermal vibration of a cantilever or tip adhesion to the surface. For enhancing Q in liquid, various cantilever geometries have been explored.[16] However, a geometry giving a high Q factor tends to provide a high k[17] and hence the obtained F_{min} is not significantly improved. Therefore, enhancement of f_0 is the most effective way to improve F_{min} without deteriorating the applicability.

To enhance f_0 without changing other parameters, we should reduce the cantilever size. The effectiveness of the size reduction has been well known since the early stage of AFM development. Nevertheless, small cantilevers have not been commonly used for atomic-scale AFM experiments in liquid. This is not only due to the difficulties in their mass production but also due to the lack of AFM instruments that can achieve the optimal performance predicted by Eq. (1) with a small cantilever.

Owing to the development of microfabrication technologies, it has recently become possible to produce small cantilevers with an acceptable yield rate.[19–21] Now, small cantilevers with a megahertz-order resonance frequency are commercially available. Figure 1(a) shows a scanning electron microscopy (SEM) image of a typical cantilever (Nanoworld NCH) that has often been used for atomic-resolution AFM imaging in liquid. The cantilever has f_0, k, and Q of 150 kHz, 40 N/m, and 8 in liquid, respectively. Figure 1(b) shows an SEM image of a small cantilever (Nanoworld USC) that has recently become available as a commercial product. The cantilever has f_0, k, and Q of 3.5 MHz, 30 N/m, and 7 in liquid, respectively. From these values and Eq. (1), F_{min} values for the NCH and USC are 4.2 and 0.8 pN at $B = 100$ Hz, respectively. Thus, the small cantilever should provide five fold improvement in F_{min} in liquid.

However, this is true only when F_{min} is predominantly determined by the thermal cantilever vibration. In practice, obtaining the thermal-noise-limited performance with a small cantilever imposes stringent requirements on AFM instrumentation. In the rest of this section, we review major problems in using a small cantilever (USC) and their solutions.

2.2 Cantilever deflection sensor

To detect the cantilever vibration at 3.5 MHz, the cantilever deflection sensor should have a bandwidth wider than at least 5 MHz. For a deflection sensor using the optical beam deflection method, we also need a high-magnification optics to align the laser beam position to the cantilever end. Moreover, noise from the deflection sensor should be very small. The optimal F_{min} is ultimately determined by the thermal cantilever vibration spectral density around f_0 ($n_z(f_0)$), which is given by

$$n_z(f_0) = \sqrt{\frac{2k_BTQ}{\pi f_0 k}}. \tag{2}$$

For a USC cantilever, this value is typically 13 fm/$\sqrt{\mathrm{Hz}}$. To achieve the thermal-noise-limited performance, noise from the deflection sensor should be much smaller than this value. To suppress the deflection noise increase due to the sensor noise to less than 10%, we should reduce its spectral density to less than 5 fm/$\sqrt{\mathrm{Hz}}$. This value is much less than a typical value for a commercial AFM system (typically > 100 fm/$\sqrt{\mathrm{Hz}}$).

Among these requirements, we can achieve the wide bandwidth and high magnification by following the standard design guidelines. On the contrary, the design of the low noise cantilever deflection sensor is not so trivial. One of the most effective solutions is

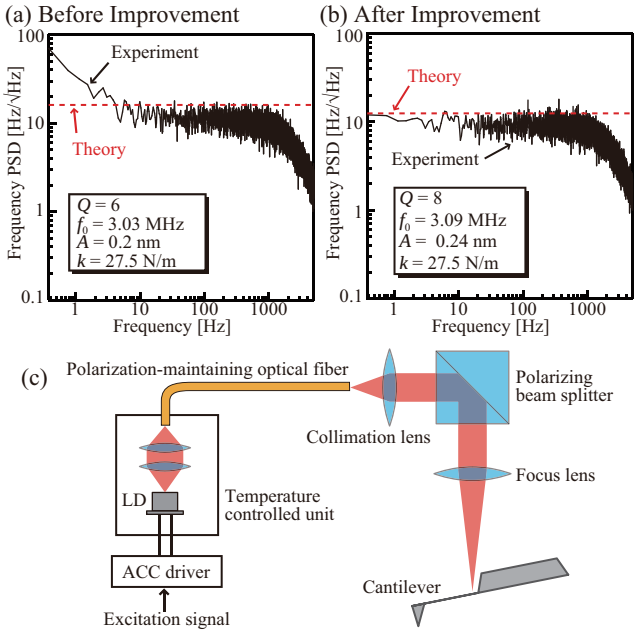

Fig. 2. (Color online) (a, b) FM spectra obtained with a USC cantilever in water before and after the improvement of the photothermal excitation setup. (c) Improved setup for the photothermal excitation. Reused with permission from Ref. 18. Copyright 2012 IOP Publishing.

the use of high-frequency laser power modulation.[22–24] By modulating the laser power at a radio frequency (300–500 MHz), we can reduce the coherence of a laser beam. In this way, we can suppress mode-hop and interference noises caused by a laser beam.

2.3 Cantilever excitation system

The piezoelectric excitation method[15] has been most commonly used for oscillating a cantilever. However, in this method, the acoustic wave generated by a piezoactuator excites spurious vibrations of various mechanical components constituting an AFM head. These spurious vibrations prevent stable and accurate measurements. To avoid this problem, we should use a direct excitation method such as the magnetic[25] or photothermal[26] excitation method. The former is not suitable for oscillating a small cantilever as the magnetic force significantly decreases when the cantilever size is reduced. The latter is the most promising candidate for oscillating a small cantilever. In this method, a laser beam with its power modulated at f_0 is irradiated to the fixed end of a cantilever. The periodically induced local thermal expansion of the cantilever material excites a cantilever oscillation.

To achieve the thermal-noise-limited performance with a small cantilever, we need to pay special attention to the stability of the excitation laser beam.[18] For example,

Fig. 2(a) shows a frequency modulation (FM) spectrum of an oscillating USC cantilever in water. The spectrum was obtained with a standard setup for the photothermal excitation. The spectrum shows an enhanced noise level in the frequency range less than 10 Hz. Such an instability is a serious problem in many of the practical AFM applications.

To suppress the instability, it is effective to improve the laser pointing stability. For this purpose, we integrated a laser diode in a temperature-controlled unit [Fig. 2(c)].[18] The emitted light is transmitted through a polarization-maintaining optical fiber to the AFM head. A polarization-maintaining optical fiber is known to provide a high immunity to temperature drifts and mechanical vibrations. Figure 2(b) shows an FM spectrum of an oscillating USC cantilever measured with the improved setup. The spectrum shows that the low-frequency noise is well suppressed to provide the theoretically expected noise level indicated by the dotted line.

2.4 EBD tips

As we reduce the cantilever size, we should also reduce the tip size. However, the conventional tip fabrication method using a Si etching process is not necessarily ideal for fabricating such a small tip. As an alternative method, electron beam deposition (EBD) of a carbon tip has been studied.[27–33] In this method, a focused electron beam is irradiated to the cantilever end by SEM. This induces deposition of decomposed organic molecules in the SEM chamber and produces a sharp carbon tip. An EBD tip is made of high-density carbon, which has Young's modulus of up to 800 GPa. This value is much larger than that of Si ($<$ 190 GPa). This difference becomes important as the tip size decreases or the scanning speed increases.

Although EBD tips have been successfully used for some of the AFM applications,[35,36] their use in atomic-scale measurements in liquid has been hindered by the following problems: An EBD tip can produce carbon contaminations, which often prevents atomic-scale imaging in liquid. The contaminations are produced either by dissolution of an EBD tip or desorption of carbon contaminations deposited on the cantilever surface during the tip fabrication process. Figure 3(a) shows an FM-AFM image of a cleaved mica surface obtained in phosphate-buffered saline (PBS) solution using a USC cantilever. The image was obtained 30 min after the immersion of a cantilever into the liquid. The large corrugation shows that the surface is covered with contaminations from the cantilever.

In our previous study,[37] we found that this problem can be solved by coating the

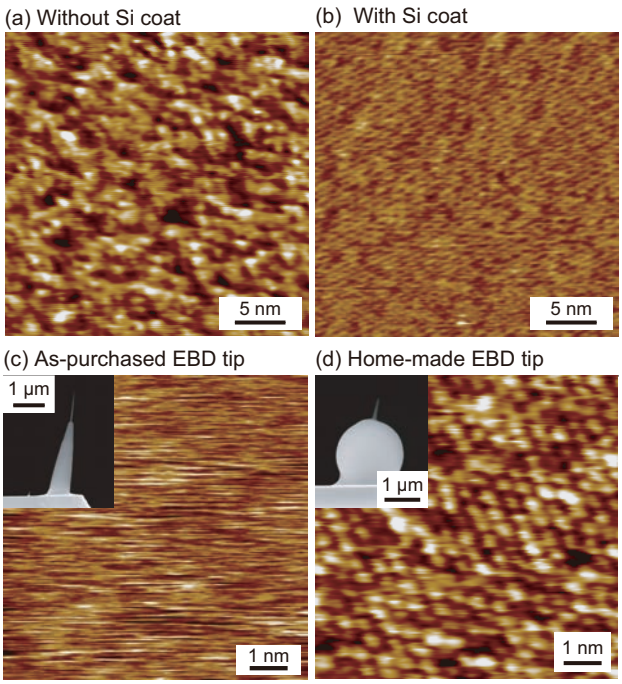

Fig. 3. (Color online) FM-AFM images of a cleaved mica surface obtained in PBS solution using a USC cantilever. (a) Without Si coat 30 min after the tip immersion into the imaging solution. (a) With Si coat 200 min after the tip immersion into the imaging solution. (c) As-purchased EBD tip with Si coat. (d) Home-made EBD tip with Si coat. Reused with permission from Ref. 34. Copyright 2015 IOP Publishing.

tip and cantilever surfaces with Si [Fig. 3(b)]. This prevents both the dissolution of the tip and the desorption of the contaminations from the cantilever surface. However, even with a Si coat, some of the EBD tips do not allow us to perform atomic-resolution imaging as shown in Fig. 3(c). As indicated in the inset of the figure, an EBD tip has a high aspect ratio. Thus, the mechanical stability is often insufficient for providing the required stability of the tip apex. To solve this problem, we developed a method for fabricating an EBD tip suitable for atomic-scale imaging in liquid [Fig. 3(d)]. In this method, we attach a 2 μm silica bead to the cantilever surface with glue and fabricate an EBD tip on it. As the tip length decreases, the distance between the cantilever and the sample during AFM experiments decreases. With decreasing cantilever-sample distance, hydrodynamic damping caused by liquid confinement between two plates becomes evident. This leads to a reduction in Q factor and hence an increase in F_{min} [see Eq. (1)]. In the proposed method, owing to the bead height, we can suppress such a cantilever-sample interaction even with a relatively short (500–700 nm) tip having sufficient mechanical strength. Therefore, we can reproducibly perform atomic-resolution

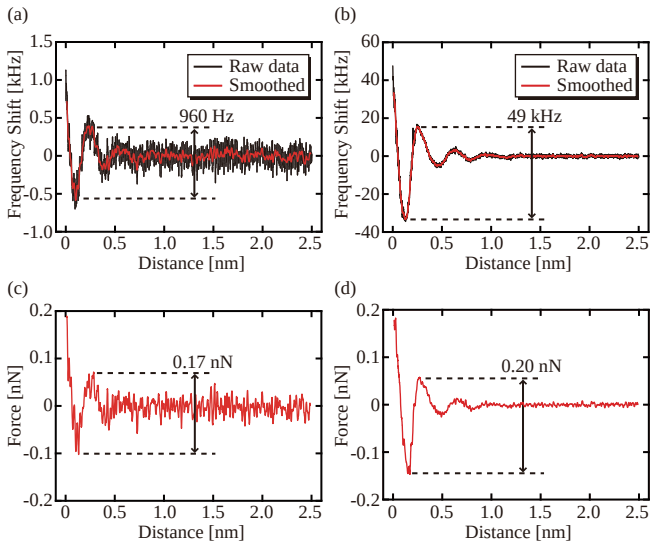

Fig. 4. (Color online) (a) (b) Frequency shift versus distance curves measured on a cleaved mica surface in PBS solution with NCH and USC cantilevers, respectively. Sampling rate: 2 kHz. Tip velocity: 1 nm/s. $B = 100$ Hz. (c) (d) Force versus distance curves calculated from the frequency shift curves shown in (a) and (b), respectively. Reused with permission from Ref. 18. Copyright 2012 IOP Publishing.

imaging in liquid with a fabricated EBD tip as shown in Fig. 3(d).

2.5 Improved force sensitivity

Figures 4(a) and 4(b) show frequency shift versus distance curves obtained on a cleaved mica surface in PBS solution using the NCH and USC cantilevers, respectively. Both curves show oscillatory profiles, reflecting the hydration structure at the mica-water interface. However, the signal-to-noise ratio (SNR) is greatly improved by the use of a small cantilever. The peak-to-peak frequency shift variation obtained with the NCH cantilever is 960 Hz, while that obtained with the USC cantilever is 49 kHz. Figures 4(c) and 4(d) show force curves converted from the frequency shift curves shown in Figs. 4(a) and 4(b), respectively. The curves show that the peak-to-peak force variations obtained with the NCH and USC cantilevers are 0.17 and 0.2 nN, respectively. From these values, we calculated force sensitivities and obtained 5.65 and 245 THz/N for the NCH and USC cantilevers, respectively. These results show that the small cantilever enhances the force sensitivity 43 times. With $B = 100$ Hz, frequency noise values are 60.4 and 354 Hz for the NCH and USC cantilevers, respectively. Thus, F_{min} values are 10.7 and 1.44 pN for the NCH and USC cantilevers, respectively. These results show that we can improve F_{min} by a factor of seven using a small cantilever. This significant improvement should

provide a sufficient force sensitivity in most of the practical applications.

3. Improvement of operation speed

Development of a high-speed atomic-resolution AFM technique requires two major improvements. First, we should improve F_{min} to achieve a force sensitivity required for true atomic-resolution imaging even with a wide measurement bandwidth B. In the previous section, we showed that we can improve F_{min} by a factor of seven using a small cantilever. Equation (1) shows that F_{min} is proportional to $\sqrt{B}$. Thus, the seven fold improvement in F_{min} creates a sensitivity margin that can be used for enhancing B 50 times without losing the capability of true atomic-resolution imaging.

Secondly, to take advantage of the sensitivity margin, we should improve the feedback bandwidth (B_{FB}) of the tip-sample distance regulation loop. The enhancement of B_{FB} requires improvements of all the components constituting the loop. In fact, we have improved the bandwidths of a cantilever deflection sensor,[38] a photothermal excitation system,[18,38] a scanner,[39,40] a high-voltage amplifier,[39] a feedback controller, a phase detector,[41] and a frequency detector. Among them, here we review the improvements of a scanner and a phase detector as they are typically the major limiting factors of the operation speed.

3.1 High-speed scanner

A high-speed operation of a scanner imposes two major requirements in the design. First, a scanner should have a high resonance frequency. This requirement is particularly stringent for a Z scanner. In fact, the maximum response time of an AFM system is often limited by the resonance frequency of a Z scanner. The design guideline to satisfy this requirement is simple. We should reduce the size and weight of a Z scanner. We should also keep its usability within an acceptable range. Thus, the major issue is the trade-off between the speed and the usability.

Secondly, a scanner should have a low cross-talk with the other mechanical components constituting an AFM head. Even if we drive a scanner at a frequency lower than its resonance, the acoustic wave generated by the scanner often excites vibrations of the other mechanical components. The induced vibrations disturb the motion of the scanner and hence practically limit the highest driving frequency.

To satisfy these two requirements, we used separate-type XY and Z scanners as shown in Fig. 5.[39,40] In the XY scanner, a pair of actuators is used for scanning the

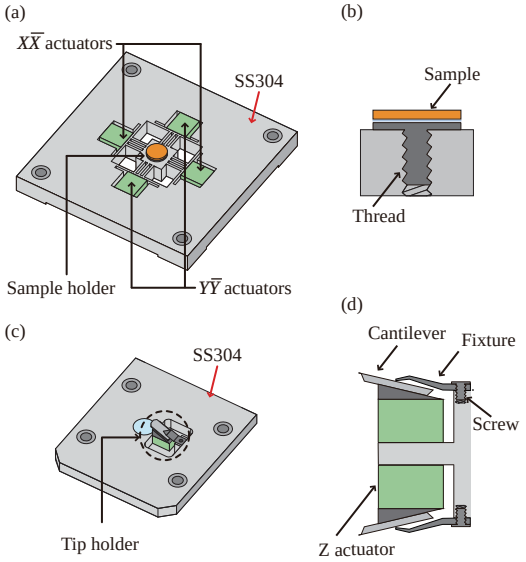

Fig. 5. (Color online) Schematic illustrations of the separate-type high-speed scanners. (a) XY sample scanner. (b) Sample holder using the screw holding mechanism. (c) Z tip scanner with a counter balance actuator. (d) Cantilever holder with a plate spring and a screw. Reused with permission from Ref. 39. Copyright 2013 AIP Publishing.

sample stage in one direction [Fig. 5(a)]. A sample is glued onto the top side of the sample holder, while a screw protruding from the bottom side of the holder is used for fixing it to the sample stage having a threaded hole at its center [Fig. 5(b)]. So far, glue has been commonly used to fix a sample holder to the stage in high-speed AFM to minimize the mass to be scanned in Z.[42] This has prevented easy exchange of samples and significantly deteriorated its usability. The screw holding mechanism allows easy replacement of samples. Owing to the separate-type design, we can use a relatively large sample (diameter $>$ 6 mm) without reducing the speed of the Z scanner.

The Z scanner consists of two actuators [Fig. 5(d)]. One of them is used for scanning the tip in Z, while the other for canceling the impulsive force generated by the scanning motion.[43] As we use an optical beam deflection sensor for detecting the cantilever deflection, the Z displacement of a cantilever caused by the scanner should change the laser spot position on the position-sensitive photodetector and hence the dc level of the cantilever deflection signal. However, this is not a serious problem in dynamic-mode AFM, where a cantilever vibration higher than 100 kHz is detected and used for the tip-sample distance regulation. The small change in dc deflection hardly influences the sensitivity of the optical beam deflection sensor. In this design, the cantilever is not glued to the stage. This also allows easy exchange of the cantilevers. These designs

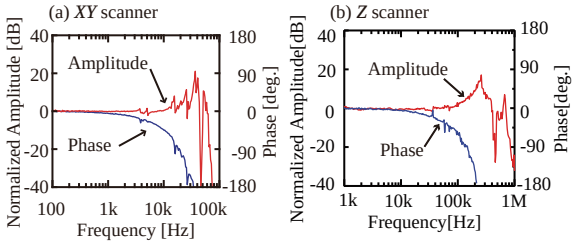

Fig. 6. (Color online) Frequency responses of (a) the XY sample and (b) Z tip scanners. Reused with permission from Ref. 39. Copyright 2013 AIP Publishing.

provide high usability as well as high resonance frequency and low cross-talk between the scanners.

Figure 6 shows frequency responses of the developed XY sample and Z tip scanners. The major resonance frequencies for the two scanners are 40 and 260 kHz, respectively. In addition, these scanners show an almost flat response up to 1 and 10 kHz, respectively. As discussed above, the sensitivity margin provided by a small cantilever allows 50 times enhancement of B without losing the atomic-resolution imaging capability. So far, typical B used for atomic-resolution imaging is $\sim$100 Hz. This suggests that we can improve B up to $\sim$5 kHz. The performance shown in Fig. 6 is sufficient for AFM operation at this bandwidth.

3.2 Low-latency phase detector

A phase detector (PD) is a key component in PM- and FM-AFMs. In PM-AFM, the phase signal is used as a feedback signal for the tip-sample distance regulation while, in FM-AFM, it is used as a feedback signal in a phase-locked loop (PLL) circuit. In both cases, the bandwidth and latency of a PD critically influence the AFM operation speed.

In a conventional AFM, a lock-in amplifier (LIA) is used for detecting the amplitude (A) and phase (ϕ) of the cantilever deflection signal [$A\cos(\omega t + \phi)$]. In the LIA, the deflection signal is multiplied by a cantilever excitation signal [$\cos(\omega t)$] to produce dc and 2ω components. The 2ω component is removed by a low-pass filter (LPF) and the dc component is used for calculating A and ϕ. However, the LPF generally has a large latency even at its pass band. This has limited the speed of the conventional PD.

Recently, we have proposed an improved method for phase detection as shown in Fig. 7.[41] In this method, instead of using the LPF for removing the 2ω component, a high-pass filter (HPF) is used for removing the dc component. The 2ω component

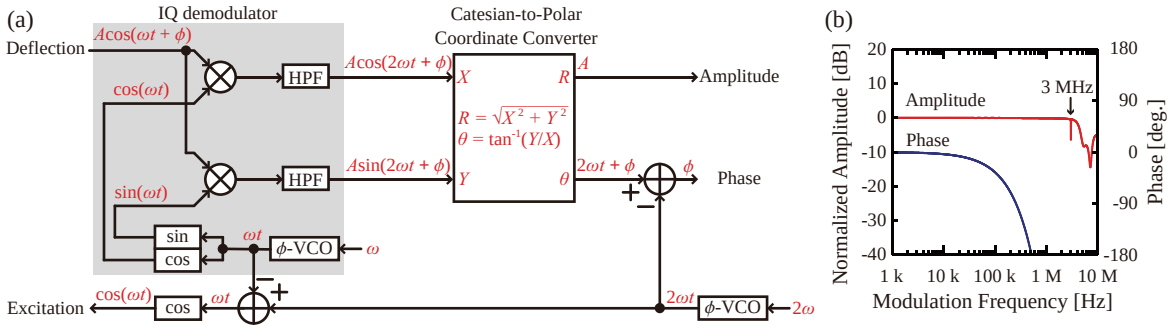

Fig. 7. (Color online) (a) Schematic diagram and (b) frequency response of the developed PD. Reused with permission from Ref. 41. Copyright 2013 AIP Publishing.

is used for calculating A and $2\omega t + \phi$. Subsequently, we can subtract the term $2\omega t$ to obtain the phase ϕ. The HPF has an almost negligible latency at its pass band, which enables high-speed phase detection.

Figure 7(b) shows the frequency response of the developed PD. We used a phase-modulated 3 MHz signal for this analysis. The amplitude response shows a flat response up to 3 MHz. Namely, the bandwidth is not limited by the PD but by the input signal frequency. However, owing to the latency of the PD, the phase response shows a gradual decrease in the frequency range higher than 10 kHz. The latency estimated from the phase curve is 0.97 μs. This performance is sufficient for achieving a B higher than 5 kHz.

3.3 Improved operation speed

We improved F_{min} using a small cantilever. We enhanced B_{FB} by improving the time response of all the devices in the tip-sample distance regulation loop. Combining all these components, we developed a high-speed and atomic-resolution AFM technique for visualizing dynamic events at a solid-liquid interface.[41)]

Figure 8 shows successive PM-AFM images of the calcite dissolution process measured in water. Atomic-scale contrasts and step edges are simultaneously visualized at 2 s/frame. This demonstrates the true atomic resolution of the developed high-speed AFM. In the imaging, the tip velocity is 10 μm/s and the periodicity of the surface corrugations is ~0.5 nm. Thus, the frequency of the corrugations to be detected (f_{cr}) is ~20 kHz. The B_{FB} of the conventional atomic-resolution AFM is less than 1 kHz. Therefore, it has been difficult to detect such a high f_{cr}. The developed high-speed AFM enables such a high-speed imaging owing to the improved F_{min} and B_{FB}.

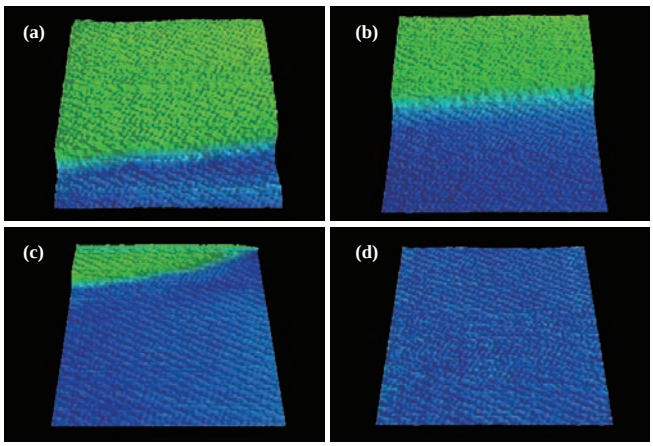

Fig. 8. (Color online) Successive PM-AFM images of calcite crystal dissolution process in water: (a) 0, (b) 20, (c) 32, and (d) 40 s. Scan size: 20 × 20 nm^2. Scan rate: 250 Hz. Imaging speed: 2 s/frame. Pixel size: 500 × 500 pix^2. Tip velocity: 10 μm/s. Reused with permission from Ref. 40. Copyright 2014 AIP Publishing.

4. Conclusions

In this review, we summarized major difficulties for improving the fundamental performance of liquid-environment atomic-resolution AFM. We reduced F_{min} using a small cantilever. We enhanced B_{FB} using a separate-type high-speed scanner and a low-latency phase detector. Combining all these efforts, we demonstrated real-time imaging of the calcite dissolution process with true atomic resolution.

To date, the difficulties in the direct imaging of solid-liquid interfacial phenomena have hindered atomic-level understanding of important issues in biology, chemistry, and physics. The development of the high-speed and atomic-resolution AFM should present a breakthrough in many of the research subjects that are related to hydration phenomena.

Acknowledgments

This work was supported by JSPS KAKENHI (25706023), and ACT-C, Japan Science and Technology Agency.

References

1) G. Binnig, C. F. Quate, and C. Gerber, Phys. Rev. Lett. **56**, 930 (1986).
2) F. Ohnesorge and G. Binnig, Science **260**, 1451 (1993).
3) T. Fukuma, K. Kobayashi, K. Matsushige, and H. Yamada, Appl. Phys. Lett. **87**, 034101 (2005).
4) T. Fukuma, J. I. Kilpatrick, and S. P. Jarvis, Rev. Sci. Instrum. **77**, 123703 (2006).
5) K. Voïtchovsky, J. J. Kuna, S. A. Contera, E. Tosatti, and F. Stellacci, Nat. Nanotechnol. **5**, 401 (2010).
6) F. J. Giessibl, H. Bielefeldt, S. Hembacher, and J. Mannhart, Appl. Surf. Sci. **140**, 352 (1999).
7) B. W. Hoogenboom, H. J. Hug, Y. Pellmont, S. Martin, P. L. T. M. Frederix, D. Fotiadis, and A. Engel, Appl. Phys. Lett. **88**, 193109 (2006).
8) M. Higgins, M. Polcik, T. Fukuma, J. Sader, Y. Nakayama, and S. P. Jarvis, Biophys. J. **91**, 2532 (2006).
9) T. Fukuma, M. J. Higgins, and S. P. Jarvis, Biophys. J. **92**, 3603 (2007).
10) H. Yamada, K. Kobayashi, T. Fukuma, Y. Hirata, T. Kajita, and K. Matsushige, Appl. Phys. Express **2**, 095007 (2009).
11) T. Fukuma, Y. Ueda, S. Yoshioka, and H. Asakawa, Phys. Rev. Lett. **104**, 016101 (2010).
12) K. Kobayashi, N. Oyabu, K. Kimura, S. Ido, K. Suzuki, T. Imai, K. Tagami, M. Tsukada, and H. Yamada, J. Chem. Phys. **138**, 184704 (2013).
13) H. Asakawa, S. Yoshioka, K. Nishimura, and T. Fukuma, ACS Nano **6**, 9013 (2012).
14) T. R. Albrecht, P. Grütter, D. Horne, and D. Ruger, J. Appl. Phys. **69**, 668 (1991).
15) Y. Martin, C. C. Williams, and H. K. Wickramasinghe, J. Appl. Phys. **61**, 4723 (1987).
16) S. Basak, A. Raman, and S. V. Garimella, J. Appl. Phys. **99**, 114906 (2006).
17) F. J. Giessibl, Appl. Phys. Lett. **76**, 1470 (2000).
18) T. Fukuma, K. Onishi N. Kobayashi, A. Matsuki, and H. Asakawa, Nanotechnology **23**, 135706 (2012).
19) M. B. Viani, T. E. Schäffer, A. Chand, M. Rief, H. E. Gaub, and P. K. Hansma,

J. Appl. Phys. **86**, 2258 (1999).

20) S. Hosaka, K. Etoh, A. Kikukawa, H. Koyanagi, and K. Itoh, Microelectron. Eng. **46**, 109 (1999).

21) J. L. Yang, M. Despont, U. Drechsler, B. W. Hoogenboom, P. L. T. M. Frederix, S. Martin, A. Engel, P. Vettiger, and H. J. Hug, Appl. Phys. Lett. **86**, 134101 (2005).

22) M. Ojima, A. Arimoto, N. Chinone, T. Gotoh, and K. Aiki, Appl. Opt. **25**, 1404 (1986).

23) A. Arimoto, M. Ojima, N. Chinone, A. Oishi, T. Gotoh, and N. Ohnuki, Appl. Opt. **25**, 1398 (1986).

24) T. Fukuma, M. Kimura, K. Kobayashi, K. Matsushige, and H. Yamada, Rev. Sci. Instrum. **76**, 053704 (2005).

25) S. P. Jarvis, A. Oral, T. P. Weihs, and J. B. Pethica, Rev. Sci. Instrum. **64**, 3515 (1993).

26) N. Umeda, S. Ishizaki, and H. Uwai, J. Vac. Sci. Technol. B **9**, 1318 (1991).

27) Y. Akama, E. Nishimura, and A. Sakai, J. Vac. Sci. Technol. A **8**, 429 (1990).

28) T. Fujii, M. Suzuki, M. Miyashita, M. Yamaguchi, T. Onuki, H. Nakamura, and T. Matsubara, J. Vac. Sci. Technol. B **9**, 666 (1991).

29) K. L. Lee, D. W. Abraham, F. Secord, and L. Landstein, J. Vac. Sci. Technol. B **9**, 3562 (1991).

30) H. Ximen and P. E. Russell, Ultramicroscopy **42**, 1526 (1992).

31) M. Yamaki, T. Miwa, H. Yoshimura, and K. Nagayama, J. Vac. Sci. Technol. B **10**, 2447 (1992).

32) M. Wendel, H. Lorenz, and J. P. Kotthaus, Appl. Phys. Lett. **67**, 3732 (1995).

33) J. H. Kindt, G. E. Fantner, J. B. Thompson, and P. K. Hansma, Nanotechnology **15**, 1131 (2004).

34) K. Miyazawa, H. Izumi, T. Watanabe-Nakayama, H. Asakawa, and T. Fukuma, Nanotechnology **26**, 105707 (2015).

35) T. Ando, T. Uchihashi, and T. Fukuma, Prog. Surf. Sci. **83**, 337 (2008).

36) N. Kodera, D. Yamamoto, R. Ishikawa, and T. Ando, Nature **468**, 72 (2010).

37) S. M. R. Akrami, H. Nakayachi, T. Watanabe-Nakayama, H. Asakawa, and T. Fukuma, Nanotechnology **25**, 455701 (2014).

38) T. Fukuma, Rev. Sci. Instrum. **80**, 023707 (2009).

39) K. Miyata, S. Usho, S. Yamada, S. Furuya, K. Yoshida, H. Asakawa, and

T. Fukuma, Rev. Sci. Instrum. **84**, 043705 (2013).

40) S. M. R. Akrami, K. Miyata, T. Watanabe-Nakayama, H. Asakawa, and T. Fukuma, Rev. Sci. Instrum. **85**, 126106 (2014).

41) K. Miyata, H. Asakawa, and T. Fukuma, Appl. Phys. Lett. **103**, 203104 (2013).

42) T. Uchihashi, N. Kodera, and T. Ando, Nat. Protoc. **7**, 1193 (2012).

43) T. Ando, N. Kodera, E. Takai, D. Maruyama, K. Saito, and A. Toda, Proc. Natl. Acad. Sci. U.S.A. **98**, 12468 (2001).